CHEMISTRY & SUSTAINABILITY

CHEMSUSCHEM

ENERGY & MATERIALS

Accepted Article

Title: Manipulating the optical properties of carbon dots via fine tuning their structural features

Authors: Hui Luo, Nikolaos Papaioannou, Enrico Salvadori, Maxie Roessler, Gereon Ploenes, Ernst R. H. van Eck, Liviu Tanase, Jingyu Feng, Yiwei Sun, Yan Yang, Mohsen Danaie, Ana Belem Jorge Sobrido, Andrei Sapelkin, James Durrant, Stoichko D. Dimitrov, and Maria-Magdalena Titirici

To be cited as: *ChemSusChem* 10.1002/cssc.201901795

Link to VoR: http://dx.doi.org/10.1002/cssc.201901795

A Journal of

ChemPubSoc Europe

WILEY-VCH

www.chemsuschem.org

Manipulating the optical properties of carbon dots via fine tuning their structural features

Hui Luo, [a,b] Nikolaos Papaioannou,[d] Enrico Salvadori,[e,f] Maxie Roessler,[e,g] Gereon Ploenes,[h] Ernst R. H. van Eck,[h] Liviu Tanase,[i] Jingyu Feng,[a] Yiwei Sun,[d] Yan Yang,[a] Mohsen Danaie,[j] Ana Belem Jorge Sobrido,[b] Andrei Sapelkin,[d] James Durrant,[k] Stoichko D. Dimitrov*[c] and Maria-Magdalena Titirici*[a,b]

Abstract

As a new class of sustainable carbon material, the term “carbon dots” represents an “umbrella term” as there are many types of materials included. We employ a broad range of techniques to develop understanding on hydrothermally synthesized carbon dots and show how fine tuning the structural features using simple reduction/oxidation reactions can drastically affect their excited state properties. Structural and spectroscopic studies found that photoluminescence originates from direct excitation of localized fluorophores involving oxygen functional groups, while the excitation at graphene-like features leads to ultrafast phonon-assisted relaxation and largely quenches the fluorescent quantum yields. This is arguably the first to identify the dynamics of photoluminescence including Stokes’ shift formation, allowing us to fully resolve the relaxation pathways in these carbon dots. The comprehensive investigation sheds light on how understanding the excited state relaxation processes in different carbon structure is crucial for tuning the optical properties for any potential commercial applications.

[a] H. Luo, J. Feng, Prof. M. M. Titirici
Department of Chemical Engineering, Imperial College London
London, SW7 2AZ, UK
m.titirici@imperial.ac.uk
[b] H. Luo, Y. Yang, Dr. A Sobrido, Prof. M. M. Titirici
School of Engineering and Materials Science, Queen Mary University of London
London, E1 4NS, UK
[c] Dr. S. D. Dimitrov
SPECIFIC IKC, College of Engineering, Swansea University
Swansea, SA2 7AX, UK
Stoichko.dimitrov@swansea.ac.uk
[d] Dr. N. Papaioannou, Dr. Y. Sun, Dr. Sapelkin
School of Physics and Astronomy, Queen Mary University of London
London, E1 4NS, UK
[e] Dr. E. Salvadori, Dr. M. Roessler
School of Biological and Chemical Sciences, Queen Mary University of London
London, E1 4NS, UK
[f] Dr. E. Salvadori
Department of Chemistry and NIS Centre, University of Turin
Turin, 10125, Italy
[g] Dr. M. Roessler
Department of Chemistry and Centre for Plastic Electronics
Imperial College London
London, SW7 2AZ, UK
[h] Gereon Ploenes, Dr. Ernst R. H. van Eck
Magnetic Resonance Research Center, Institute for Molecules and Materials, Radboud University
Nijmegen, 6525 AJ, Netherlands
[i] Dr. L. Tanase
National Institute of Materials Physics
Magurele-Ilfov, 077125, Romania
[j] Dr. M. Danaie
Diamond Light Source Ltd., electron Physical Science Imaging Centre
Harwell Science and Innovation Campus, Didcot OX11 0DE, UK
[k] Prof. J. Durrent
Department of Chemistry and Centre for Plastic Electronics
Imperial College London
London SW7 2AZ, UK

Supporting information for this article is given via a link at the end of the document.

Introduction

Carbon dots (CDs) is the generic name for a class of low-cost carbon nanomaterials, firstly reported in 2004,[1] possessing photoluminescent (PL) properties with an average particle size below 10 nm.[2] This category of carbonaceous materials is attractive for many applications ranging from bio-imaging to sensors, optoelectronics and more[3–7] due to their facile and inexpensive synthesis, low toxicity,[6] high (aqueous) solubility, optoelectronic properties, facile modification and stability against photo-bleaching.[8] Current synthetic approaches to produce CDs include top-down and bottom-up methods, which usually give aggregated graphene-like layers of various size and a large structural diversity including sp^2 / sp^3 carbon networks and oxygen rich functional groups at different ratios.[9] As a result, the photoluminescence properties of CDs widely vary in quantum yields, from < 1 % to 95 % depending upon synthesis. Light excitation wavelength dependent and independent emission have also been widely reported.[10–13] Experimental and theoretical studies of CDs have revealed that photoluminescence originates predominantly from π-π* transitions involving hybridized orbitals from the sp^2 carbon core (amorphous and nanocrystalline) and functional C=O and COOH and C-O-C groups.[14,15] Radiative n-π* transitions involving carbon-oxygen surface groups are also thought to contribute to emission and can explain the observed solvent polarity and surface functionalization effects on light absorption and emission.[16,17] In addition, quantum confinement,[18] carbon cluster agglomeration and the formation of supramolecular aggregates[19] have also been reported demonstrating the great complexity of their optical absorption and emission properties and the need for fundamental studies to unlock their potential for semiconductor-like and biological applications.[20]

In this work, we focused on a specific member of the CDs family, namely CDs prepared via Hydrothermal Carbonization (HTC) of carbohydrates from natural products.[21,22] In HTC, carbohydrates are converted into micrometer-sized carbonaceous spheres via

a process involving 5-hydroxymethylfurfural (5-HMF) formation, its "polymerization" via a nucleation-growth process and intermolecular dehydration. Simultaneously to the formation of the micrometer sized-sphere sediments in the aqueous phase, there is also a formation of CDs with a diameter of a few nanometers which have been shown to have crystalline domains despite the low carbonization temperatures. By treating these CDs isolated from the aqueous phase of the HTC process with oxidization and reduction agents, we induced changes in the crystalline structure and functional groups, which changed their optical properties. These steps were deliberately designed to create more graphene-like CDs with a lower density of oxygen functional groups in the reduced samples (r-CDs) and highly amorphous CDs with a higher density of oxygen motifs in the oxidized samples (o-CDs). The structures of the CDs were analyzed using several structural techniques including HR-TEM, EPR, XPS, Raman, ^{13}C-NMR and FTIR which allowed us to build a detailed picture of the structure and chemistry of the CDs. Then, the photoluminescence properties of the CDs were studied and it was found that they vary significantly between samples, with o-CDs showing enhanced PL while r-CDs showing much weaker PL. These differences were analyzed using femtosecond transient absorption (TA) spectroscopy and time-correlated single photon counting (TCSPC) which identified that the time scale of non-radiative excited state relaxation causing to PL quenching is picoseconds and that this quenching is mostly determined by the proportion of C-O versus C=C carbon in the dots.

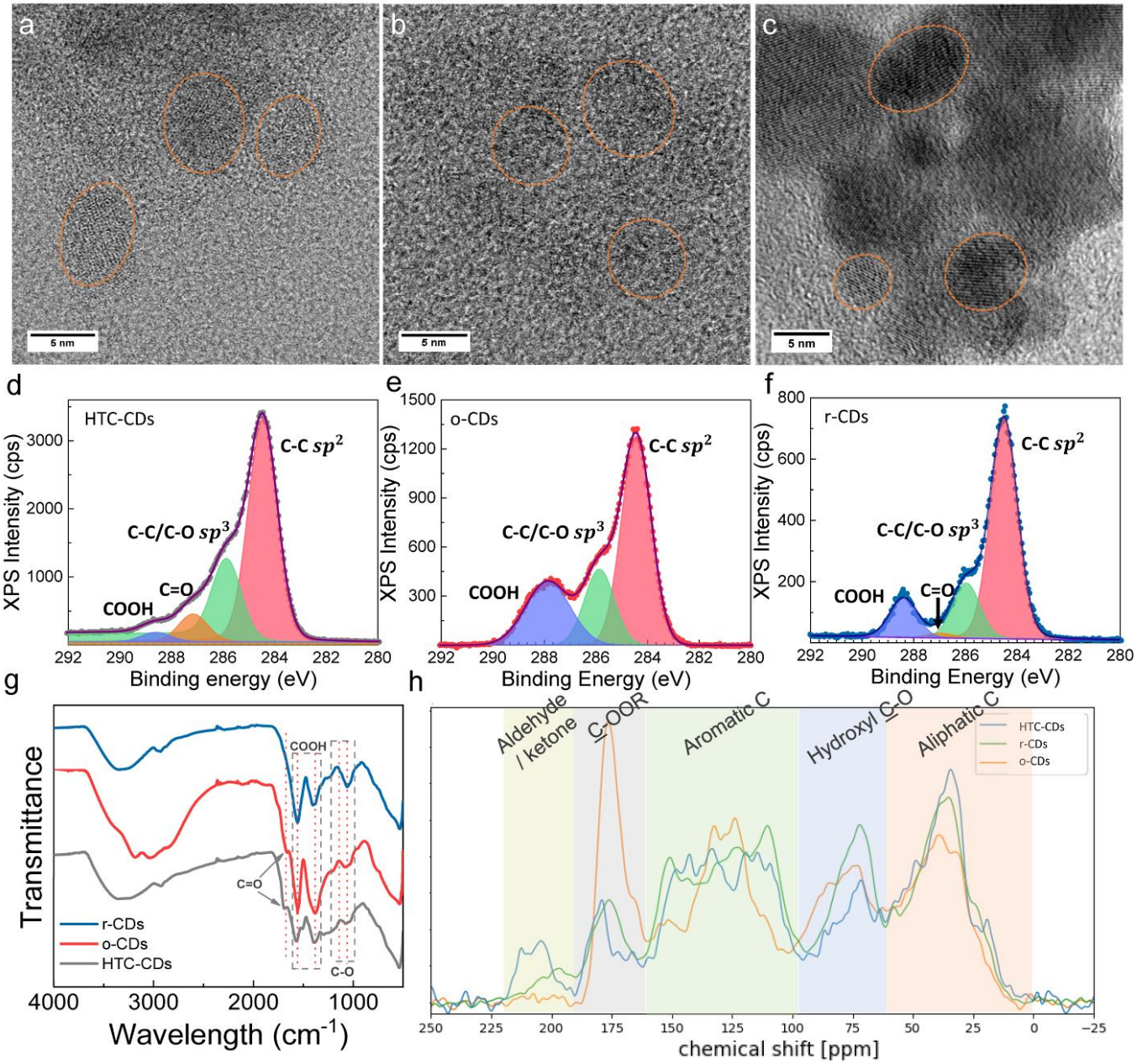

Figure 1. HR-STEM bright field images taken at 80 kV and C1s XPS spectra of (a, d) HTC-CDs, (b, e) o-CDs and (c,f) r-CDs; (g) corresponding FTIR spectra; (h) Solid state CP-MAS ^{13}C NMR spectra.

Results and Discussion

CDs were prepared via hydrothermal carbonization (HTC) of glucose,[23] by treating a 4% w/v aqueous glucose solution at 200 °C for 12 hours, followed by centrifugation and filtration to isolate the CDs from the larger carbon microspheres which simultaneously form during this process as explained above. The as-prepared CDs, named HTC-CDs here, appear as a yellow aqueous suspension that shows visible blue emission (around 450 nm) when illuminated by UV light. The HTC-CDs were then treated with oxidation (H_2O_2 / NH_4OH) and reduction ($NaBH_4$) agents for structural and optical studies, and the products are denoted as o-CDs and r-CDs, respectively. The o-CDs appear as a light-yellow solution while r-CDs show brown color with the same concentration, both of which emit blue-green light upon UV excitation. The details regarding the preparation methods can be found in the experimental section.

Morphological characterization (Figure 1a, b, c) by high-resolution scanning transmission electron microscopy (HR-STEM) bright field images indicates that the as prepared HTC-CDs are about 5 nm in size and contain small lattice fragments embedded in an amorphous carbon matrix (Figure S1). Although the o-CDs and r-CDs have similar particle sizes, differences in the structure can be observed with o-CDs exhibiting more amorphous features and a higher degree of disorder, while the r-CDs showing more graphitic features with lattice fringes spaced by 0.24-0.29 nm which corresponds to the (001) crystal plane of graphite.[3] The different lattice spacing observed in the same sample implies the inhomogeneity of the carbon core structure, which would be further verified in the more detailed structural analysis later.

Despite of the morphological differences observed in HR-STEM, the Raman Spectra of HTC-CDs and r-CDs (acquired using 488 nm laser, Figure S2) display similar characteristics including a graphitic G band originating from the stretching of sp^2 carbon atoms and a weaker D band indicative of structural distortion of the graphitic sp^2 carbon layers with defects like sp^3 coordination or small dot size difference. A combination of Breit-Wigner-Fano (BWF) + Lorentzain line pair was used to fit the Raman spectra and the I_D/I_G ratio was calculated from the estimated peak heights (Table S1). Compared to the HTC-CDs, the D band of r-CDs broadens, whereas the G band becomes slightly narrower. The I_D/I_G ratio of r-CDs is also 53 % bigger than that in HTC-CDs. We infer the development of D peak stems from the sp^3 carbon atoms forming small aromatic clusters. Since those clusters are isolated by the amorphous matrix, the disorder increase, leading to a higher D band intensity. The Minor narrowing of the FWHM of G band shows that, whilst disorder is still high in the r-CDs, these dots have an increased uniformity of the sp^2 graphitic nature.[24]

Table 1. Chemical composition of HTC-CDs, o-CDs and r-CDs extracted from the XPS data in **Figure 1**.

Sample	C-C sp^2	C-C/C-O sp^3	C=O	COOH
HTC-CDs	66%	23%	8%	3%
o-CDs	55%	20%	< 1%	25%
r-CDs	69%	17%	2%	12%

The XPS spectra of the CDs are presented in Figure 1d, e, f and their estimated bond compositions presented in Table 1. The XPS results identify that r-CDs have the highest percentage of sp^2 carbon among the three samples, in good agreement with our TEM and Raman analysis suggesting a more graphitic core structure of the r-CDs than the other two CD types. HTC-CDs have slightly lower ratio of sp^2 carbon than r-CDs whilst o-CDs show only 55% of sp^2 carbon. On the contrary, the oxygen content in o-CDs has dramatically increased compare to HTC-CDs and r-CDs, indicating a more oxidized state. More COOH groups have also been detected in r-CDs, whose formation will be explained later at the solid state ^{13}C NMR part. Detailed O1s spectra can be found in Figure S3.

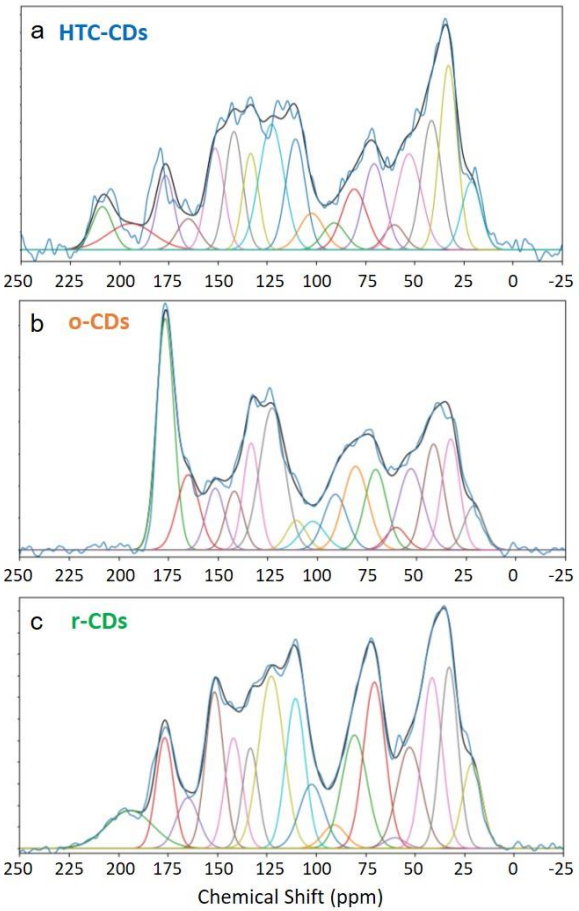

Figure 2. Peak fitted ^{13}C-NMR spectra of (a) HTC-CDs, (b) o-CDs and (c) r-CDs.

Structural evidence of the different functionalization level can also be found from infrared (IR) spectroscopy, Figure 1g, where two major peaks for the symmetric and antisymmetric stretches at 1569 cm^{-1} and 1376 cm^{-1} are assigned to COOH surface

functionality.[25] Sub-peaks beside the two COOH peaks in HTC-CDs indicate there are other chemical bonds, but have been removed by the post-treatments. Two additional shoulder peaks at 1700 cm^{-1} are present in HTC-CDs and o-CDs, corresponding to C=O stretches.

Solid state ^{13}C NMR analysis of CDs provides further insights on how the chemical structure of as-synthesized CDs has been altered after the oxidation/reduction treatment. Peak fitting of the spectra from HTC-CDs (Figure 2a) suggests that the main structural motif of the CDs is complex, and formed of furan molecules, linked by direct C-C bonds or involving a methine or a methylene bridge. Oxygen terminal groups such as ketone, aldehydes and carboxylic acids are linked to the structure. The furan-molecules can also condense leading to the formation of six-member-aromatic rings, as confirmed by the TEM images. The same peaks have been used to fit the spectra of the o-CDs and r-CDs. As seen from Figure 1h and 2b, a drastic increase at 175 ppm corresponding to COOH groups is noticed, while the ketone/aldehyde groups and furan rings have largely decreased, which suggests that the oxidation process further turned C=O groups into COOH, as well as opened the furan rings and formed COOH end groups, resulting in small aromatic clusters connected with carboxylic acid end groups, which disrupts the carbon core structure leading to a higher disorder degree. On the contrary in the r-CD spectrum (Figure 2c), most of the C=O groups have been reduced to C-OH, as suggested by the peak increase at 75 ppm. The relative quantities in the individual peaks (Figure S4) indicate the increase in aromatic rings in the r-CD backbone structure and the decrease of oxygen motifs, in perfect agreement with our XPS and FTIR analyses. The different arrangement of the aromatic rings might cause the different local crystalline structure as we see in the microscopy images. The higher content of COOH groups in r-CDs are likely to be due to the opening of furan rings as observed in o-CDs. Since $NaBH_4$ is not strong enough to reduce COOH groups, the presence of carboxyl groups remained in the r-CDs structure.

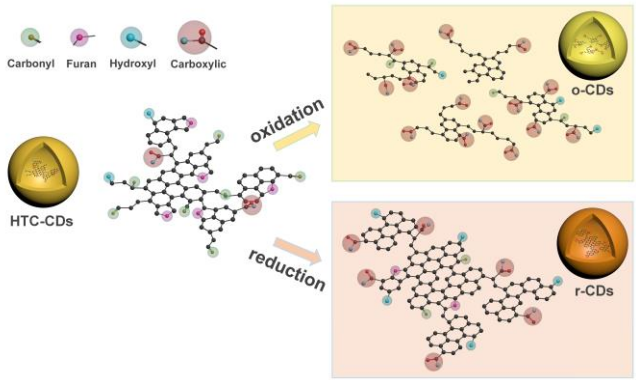

Scheme 1. Schematic diagram describing the structure evolution of carbon dots.

The differences in the structure and functionalities between the samples confirm that chemical oxidation and reduction tune the structure of hydrothermal CDs. Based upon our structural analysis, we can draw a representative scheme of the HTC-CDs, r-CDs and o-CDs, shown in Scheme 1. Upon the oxidation of HTC-CDs, furan rings in the carbon base structure opened up to form COOH end groups, resulting in a highly disordered core structure. Upon reduction of HTC-CDs, the density of sp^2 carbon is increased creating r-CDs with a more extensive conjugated aromatic carbon network[26] and smaller density of oxygen groups. The HTC-CDs show "an in between" scenario where they have a moderate C/O ratio and C=O/COOH content.

Figure 3a presents the UV-Vis absorbance spectra of HTC-CDs, r-CDs, and o-CDs dispersed in water with a concentration of 0.1 mg/ml. Each sample has a spectrum with a strong absorption towards the UV which tails off in the visible range.[27–29] The spectra show discernible differences between the samples signifying the impact of chemical reduction and oxidation on the optical properties of CDs. Comparing HTC-CDs to o-CDs, we observe that HTC-CDs display a clear peak at 295 nm (λ_{abs}) normally attributed to π-π* transitions within the sp^2 carbon core,[30] while for o-CDs this peak disappears and absorbance intensity monotonously decreases in the visible spectral region. This absorbance change in o-CDs is caused by the partial destruction of the sp^2 hybridization network upon oxidation, which decreases the probability for π-π* transitions, in analogy to wide energy gap systems.[14,31] Compared to HTC-CDs, r-CDs have a well-defined absorption peak with a maximum at ~ 260 nm and much stronger visible absorption up to 650 nm which resembles the absorption of graphene and graphene oxide with narrow energy gaps indicating a significant contribution from conjugated domains.[32–35] The energy gap changes based on sizes of sp^2 domains can be found in previous experimental and theoretical studies.[15,19,36]

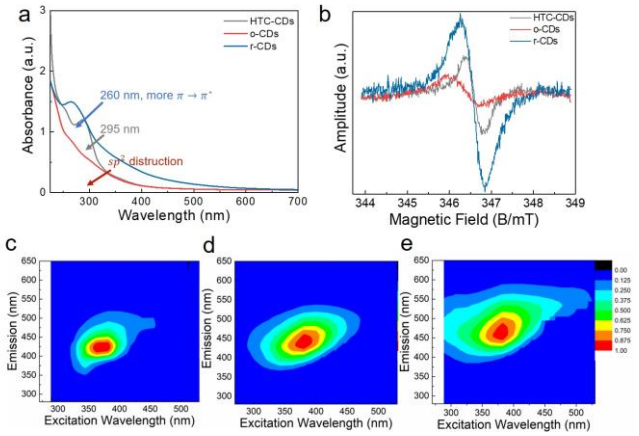

Figure 3. (a) UV-Vis absorbance of aqueous solutions of CDs (concentration: 0.1 mg/mL) and (b) EPR signal comparison of CD powders measured at room temperature; Photoluminescence maps of (c) HTC-CDs; (d) o-CDs; (e) r-CDs.

Steady-state photoluminescence measurements as a function of excitation wavelength were carried out and the 3D spectral maps are presented in Figure 3c, d, e. The excitation wavelength was increased from 250 nm to 530 nm in 20 nm

increments. Solutions for these were prepared with deionized water and concentrations were kept at 0.1 mg/ml. The CDs exhibit excitation-dependent emission spectrum, typical for CDs, which peaks in intensity at ~ 370 nm excitation (also seen in Figure S7).[16,37–40] Therefore, PL quantum yields (Φ) were recorded with a 370 nm excitation against a reference quinine sulphate solution.[41] The results show significant differences between each sample which are as follows: 1.82% for o-CD, 1.28% for HTC-CDs and 0.18% for r-CDs. The rather low quantum yield is attributed to the dopant-free hydrothermal synthesis, as heteroatom doping tends to dramatically increase the quantum yield of carbon dots. This result is consistent with some published work.[11,36,42–46] This trend in Φ is an indicator of the strong impact of chemical treatment on the optical properties of HTC-CDs. Reduction with $NaBH_4$ leads to a significant drop in Φ likely caused by the increased graphitic character of r-CDs. Oxidation with H_2O_2 / NH_4OH leads to an increase in Φ coinciding with the reduction in the amount of aromatic carbon and the increase of COOH groups in o-CDs.[47–49] A direct comparison between Φ and the dot's composition according to the XPS and NMR results shows that there is a direct correlation between the relative percentage ratio of C=O/COOH groups and Φ, indicating that the emissive excited states in the CDs synthesized here include oxygen functional groups.

Figure 3c, d, e present normalized 3D-PL plots of each of the samples studied revealing that despite of their big difference in Φ, the CDs and specifically o-CDs and r-CDs have nearly identical spectral features with a central PL peak at ~ 460 nm originating from an excitation at ~ 370 nm. This indicates that the origin of emission is from very similar excited states with an absorbance at ~ 370 nm not well-resolved in the UV-Vis absorbance spectra of the CDs and indicating a low concentration of the emissive fluorophores or low absorption coefficients. The data show that the strongest absorption < 300 nm in all CDs does not populate excited states, contributing strongly to PL. This is frequently observed for a variety of CDs and is related to their graphitic character inducing non-radiative phonon-assisted relaxation processes rather than relaxation to emissive states.[27,28] A very similar peak broadening is observed for r-CDs and o-CDs further indicating that the origin of PL is due to the same excited states comprising of a common structural motif. Based on these observations and the structural correlations with Φ therefore conclude that PL originates from structures within the dots consisting of oxygen groups. The density of these oxygen motifs is clearly higher in o-CDs than in r-CDs identifying that chemical reduction is disadvantageous for the production of strongly emissive CDs, whilst oxidation is advantageous, as seen from Figure 4f. The influence of Na^+ and NH_4^+ on HTC-CDs was also investigated; as seen in Figure S8. After adding the ions, no major changes were found in the absorption and PL spectra of the sample, indicating a negligible effect on excited state properties.

Another likely contributor to the dramatic change of quantum yield (Φ) in o-CDs and r-CDs is the presence of radicals, which are known to serve as traps for non-radiative recombination.[50,51] Continuous-wave EPR was used to obtain an estimate of the relative radical concentrations (by comparing normalized peak intensities) as well as a first indication of their chemical environment (based on the characteristic g values); Figure 3b reports experimental evidence on the three different compounds.

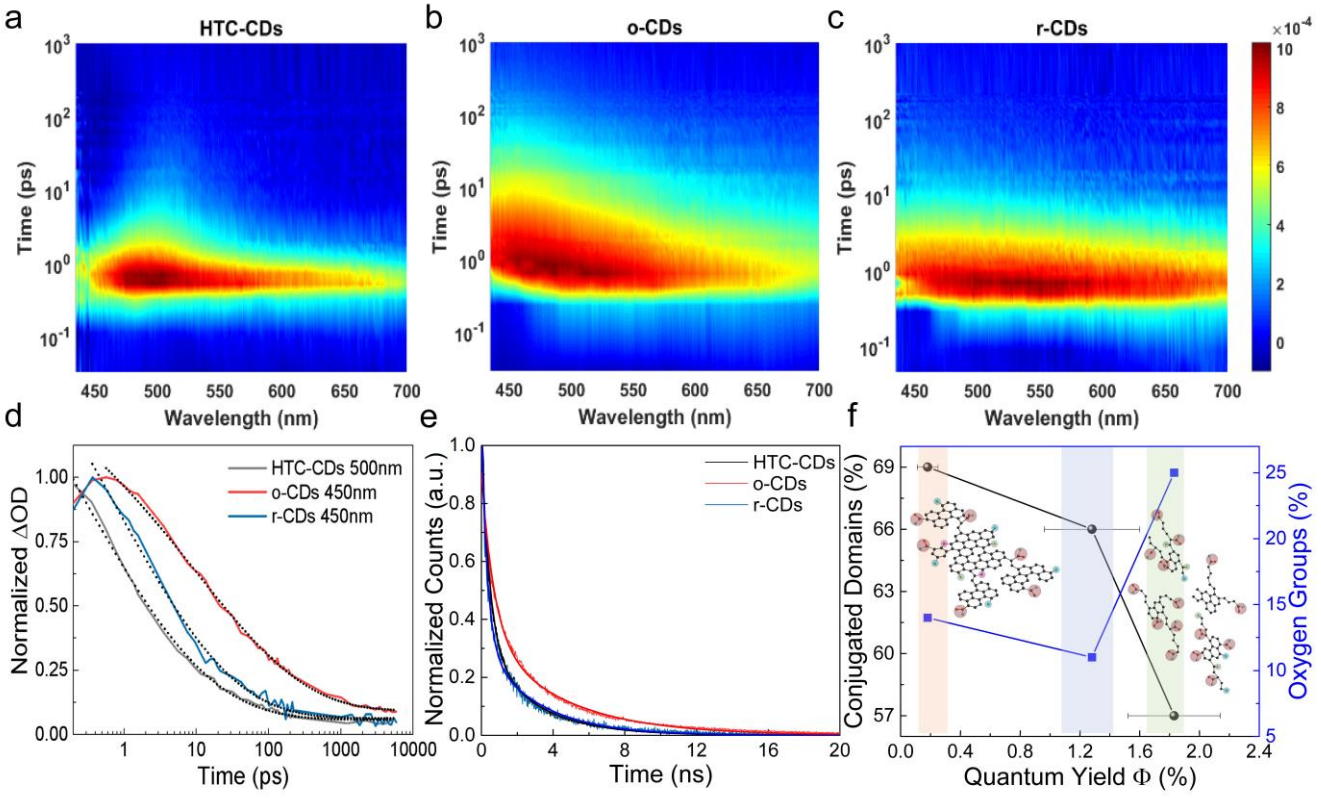

Figure 4. Femtosecond TA spectral maps of (a) o-CDs (b) r-CDs (c) HTC-CDs normalized to HTC-CDs spectra, and corresponding kinetics at (d) 450 nm for o-CDs/r-CDs, 500 nm for HTC-CDs with 360 nm pump;(e) TCSPC emission decays at 500 nm fitted with a bi-exponential function; results from fits are presented in Table 2; (f) Summarizes the interplay between quantum yield (Φ) and XPS percent density of the conjugated sp^2 carbon and oxygen contained groups.

From the intensity of the EPR spectra, after normalizing for sample mass and number of scans, the relative concentrations follow the order r-CDs > HTC-CDs >> o-CDs. On the other hand $g_{o\text{-}CDs} > g_{HTC\text{-}CDs} > g_{r\text{-}CDs} > g_e = 2.0023$ which, under the reasonable assumption that all CDs harbor π-radicals, which can be linked with paramagnetic carbon-related dangling bond centers or other structural intrinsic defects,[52,53] suggests that o-CDs radicals are more substituted with oxygen-containing groups than r-CDs due to the milder conditions (H_2O_2 and NH_4OH are both weak reacting chemicals).[54] The reduction process takes place in an alkaline environment, which can turn COOH into COO·. The removal of functional groups during reduction would also create dangling bonds, resulting in more radicals detected.[55] The ratio between $\Phi_o/\ \Phi_r$ is similar as the intensity ratio of r-CDs vs o-CDs, which offers good indication of the effect of free radicals on the PL. Akin to the case of fluorescent silicon nanocrystals, free radicals can act as surface defects and have a negative effect on PL.[51,56] A deeper insight into the chemical structure of these radicals is provided by pulse EPR experiments that measure the hyperfine coupling between electron and nuclear spins. HYSCORE experiments show an extended conjugated network in r-CDs compared to HTC-CDs around the paramagnetic defects (Figure S5 and S6), in good accordance with bulk spectroscopies such as NMR and FTIR that inform on the average structure of CDs. However, with current results it is hard to conclude the types of the radicals formed. More work including time-dependent EPR would be conducted in the future to understand the formation mechanism.

To gain insights on the excited state properties of the CDs, we carried out time-resolved photoluminescence and absorption spectroscopic studies. Time-correlated single photon counting (TCSPC) was used to measure the PL lifetimes of CDs by employing a 405 nm laser excitation and probing at 440, 500, 550 and 600 nm. The resulting PL decays at 500 nm are included in Figure 4e, whilst the rest are included in Figure S9. The 500 nm decays were best fitted with a bi-exponential function yielding sub-nanosecond and nanosecond time constants (Table 2), matching previously published PL lifetimes of CDs.[14,50,52] Our data show that o-CDs have the longest-lived PL whilst HTC-CDs the shortest-lived, contradicting the trend in Φ measured by us and ranking r-CDs as the least emissive system out the three studied. Similar discrepancies between lifetimes and Φ have been observed for CDs and indicate that fluorescence lifetimes on the nanosecond time scale are not fully indicative of the whole emission dynamics of HTC-CDs.[50,57,58] Possible reasons for this behavior include static quenching or faster picosecond non-radiative relaxation of the excited states.[50] The decays in Figure S9 show that the PL on the hundreds of picosecond and nanosecond timescales is mostly wavelength independent, supporting the conclusion that PL originates from individual excited states (fluorophores) not interacting with each other via energy or charge transfer processes,[50] and that ultrafast sub-nanosecond non-radiative recombination or ground state complexes determine the dots PL properties including their Stokes shift.[14]

Femtosecond transient absorption (TA) spectroscopy was used to shed light on the excited state dynamics in the CDs on the sub-nanosecond timescale. The samples were studied using 360 nm 100 fs laser pulses and 430-700 nm broadband probe light. Figure 4a, b, c show 3D maps of the change in absorbance (ΔA) plotted as a function of time and probe wavelength for o-CDs, r-CDs and HTC-CDs solutions, correspondingly. The excitation wavelength is 360 nm and the maps present the evolution of ΔA as a function of time up to 6 ns. The maps reveal a broad excited state absorption (ESA) signal with a distinctly different spectral shape and dynamic for each of the CDs agreeing with their different Φ and structural properties. Stimulated emission was not clearly observed due to the CD's low Φ, although such signals may be over imposed on the positive ESA.[47,52,59] From Figure 4a, we find that the ESA of o-CDs undergoes a sub-picosecond peak shift of > 0.4 eV which is followed by peak narrowing producing a low intensity signal (< 5 %) with a maximum at ~ 450 nm. This ultrafast process can be interpreted as energy transfer through a density of states or an excited state vibrational relaxation generating localized emissive excited states and causing the Stokes shift detected by our PL experiments. Such shifting and dynamics are not clearly dominant in the spectra of r-CDs and HTC-CDs, at least within our instrument response function, but instead their ESA dynamics indicates much faster excited state relaxation and a lower yield of generated long-lived localized excited states. Therefore, these data suggest that the reduced rigidity of the o-CDs compared to r-CDs and HTC-CDs and their increased concentration of oxygen groups is clearly beneficial for enhancing their Φ.

Table 2 Results from least square fitting of the transient absorption decays at 450 and 500 nm using a stretched exponential function (τ1 corresponds to the lifetime and β to the stretching exponent) and the TCSPC emission decays at 500 nm using a bi-exponential function (A_1 and A_2 are the exponential pre-factors and τ_1 and τ_2 are the lifetimes)

TAS	wavelength	τ_1 (ps)	β
HTC-CDs	500 nm	0.20	0.23
o-CDs	450 nm	9.92	0.28
r-CDs	450 nm	0.69	0.26

TCSPC	wavelength	A_1	τ_1 (ns)	A_2	τ_1 (ns)
HTC-CDs	500 nm	69%	0.46	31%	2.8
o-CDs	500 nm	62%	0.69	38%	4.28
r-CDs	500 nm	65%	0.33	35%	3.04

Unlike previous ultrafast spectroscopy studies of CDs, fitting of the ESA decay kinetics was successful both with a stretched exponential and a 3-exponential function,[14,48,60] thereby, providing little extra information about the nature of the competing relaxation processes in this system, but giving us a good indication of the average timescale of excited state decay

to compare between CDs. Table 2 presents the results from our least square fitting with the stretched exponential function $\Delta A \sim \exp(-(t/\tau)\beta$, where β is the stretching exponent, τ is the decay time constant and t is time. The results show that light absorption by o-CDs leads to a dominant ultrafast excited state decay with a τ = 9.9 ps and β = 0.28 indicating a rather large distribution of decay constants and ultrafast excited state relaxation. Such ultrafast excited state decay dynamics are typical for graphene and graphene oxide systems and recently investigated with temperature dependent PL studies in carbon triangle, all of which identify the main non-radiative relaxation mechanism to phonon-assisted relaxation to ground state through the density of states of the sp^2 carbon network.[37,48,60–62] According to our results, the non-radiative relaxation is an order of magnitude faster in r-CDs than in o-CDs agreeing with the differences in Φ between these systems and indicating that the increased graphitic structure of r-CDs is the main cause of this sample's weaker PL, consistent with other people's work.[11,36,42,43,46]

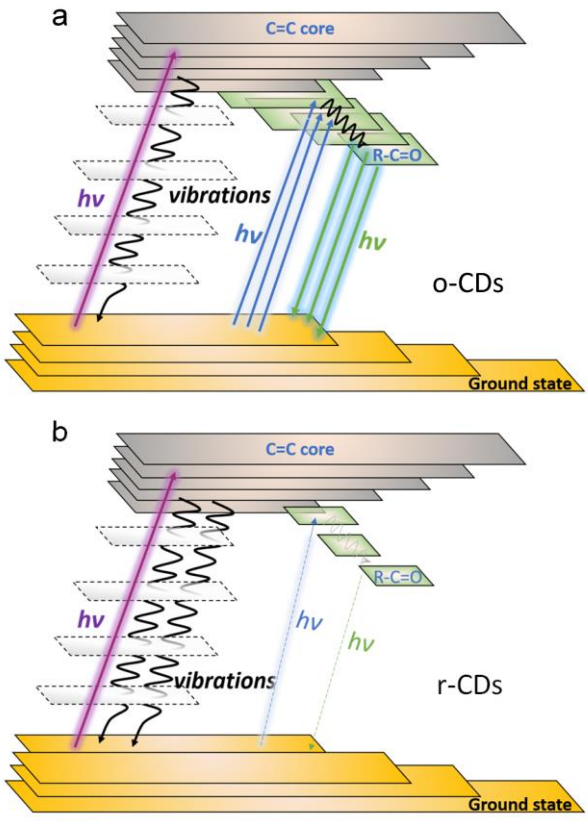

Figure 5. Excited state diagrams of (a) o-CDs and (b) r-CDs depicting the branching ratio between excited states of non-emissive sp^2 C=C graphitic carbon and emissive oxygen contained groups.

To analyze the excitation wavelength dependence in the excited state properties of the CDs, as seen from the PL spectra in Figure S7, we recorded the transient absorption spectra of the CDs using an excitation of 310 nm. Comparing between the 310 and 360 nm spectra (Figure S10), we observe that the ESA is longer lived and with less pronounced trapping into localized emissive states for the shorter wavelength excitation. This behavior supports our peak assignment of the transitions in the steady-state absorption spectra near 300 nm to predominantly π-π* transitions populating the sp^2 aromatic carbon core of the CDs, whereas excitation at longer wavelengths populates localized emissive excited states. It also shows that the interactions between these two-types of chromophores is weak and that excitation of the core states leads to ultrafast non-radiative relaxation to the ground state instead of energy transfer or internal conversion to localized emissive states. In addition, the non-radiative relaxation from the core states is slower for higher energy photon excitations as can be expected for phonon-assisted internal conversion processes.

Based on the findings from our spectroscopic study, we can propose the relaxation process diagram of the o-CDs and r-CDs (Figure 5), in which we identify that there are two main types of excited state chromophores within the CDs loosely defined as sp^2 core state and oxygen groups. The higher amount of aromatic structure in r-CDs causes excitation of the CDs to be predominantly into states delocalized over the sp^2 carbon which then leads to dominant non-radiative phonon-assisted internal conversion to the ground state resulting in the r-CDs' low Φ. In o-CDs, the ratio of sp^2 to oxygen fluorophores is smaller leading to an order of magnitude higher Φ and longer lifetimes, either of which would favor their application in photocatalytic or optoelectronic applications.[21,63–65] Considering the similarity of structural and optical properties in hydrothermally prepared carbon materials,[66–69] fine tuning their structural features with oxidation/reduction to control the optical properties should be applicable to hydrothermal CDs.

Conclusions

In this paper, the structure and surface states of hydrothermally synthesized carbon dots were altered by chemical oxidization and reduction treatments. Morphological and structural evolution studies using TEM, XPS and ^{13}C solid state NMR demonstrate that compared to the as-prepared carbon dots (HTC-CDs), the oxidized carbon dots (o-CDs) possess a more amorphous and disordered structure due to the disruption of aromatic furan rings into COOH end groups, while the reduced carbon dots (r-CDs) show more graphitic and ordered structure arising from the partial restoration of sp^2 carbon structure. The UV-Vis absorbance and photoluminescence are strongly affected by the changes in structure; specifically, o-CDs have an order of magnitude higher quantum yield than r-CDs. Despite of the difference in quantum yields, the PL profiles of o-CDs and r-CDs are similar indicating that these structurally different CDs have similar emission centers but with a different relative density. We identify that these centers act as individual chromophores on the nanosecond timescale and their excited states involve oxygen functional groups. The results from TAS and TCSPC experiments are consistent with the existence of competing ultrafast excited state relaxation processes of excited state trapping into emissive centers or relaxation to the ground state

via phonon-assisted internal conversion. The latter process is faster and more dominant in r-CDs because of their increased graphitic structure but suppressed in o-CDs allowing for excited state trapping into the emissive excited states.

This paper sheds light on the importance of investigating how fine changes in the structure of carbon dots can induce significant changes in their optical properties and can help develop simple chemical methods to tailor these properties for specific applications in bio-labelling, optoelectronics and photocatalysis. This is very important as currently in the literature, the term "carbon dots" is used very broadly which makes it rather difficult to unify these very different materials. We show that there are clear differences even within the same class of carbon dots, as exemplified here by the hydrothermally carbonized carbon dots and how understanding their detailed structure is crucial for controlling their optical properties. Future work would focus on tailoring the structure and PL performance of hydrothermal carbon dots (size, number and type of functional groups and graphitic character) for practical applications with focus on photocatalysis.

Experimental Section

Chemicals:

D-(+)-glucose, ammonium hydroxide, hydrogen peroxide, 0.5-1kD dialysis membrane, sodium borohydride, sodium hydroxide (pellets, $\geq$ 98%) are purchased from Sigma-Aldrich. hydrochloric acid (assay 36.5-38%) was purchased from VWR chemicals, quinine sulphate was purchased from Acros Oragnics. All the chemicals were used without further purification.

The preparation of CDs:

The carbon dots (CDs) were prepared by hydrothermal carbonization of D-(+)-glucose. Briefly, the precursor was dissolved in water (4% w/v) and placed in a Teflon-lined, stainless steel autoclave, which underwent treatment at 200 °C for 12 h. The obtained yellow solution was centrifuged at 10,000 rpm for 10 min to separate the liquid containing fluorescent CDs from the solid black carbonaceous precipitate. The liquid phase containing CDs was then filtered using standard syringe filters, dialyzed with 0.5-1 kD dialysis membrane and freeze dried to obtain solid CDs, which is named HTC-CDs.

A modified method for mild treatment of carbon nanotubes was used for oxidizing the carbon dots (o-CDs). Typically, 0.3 g of the as-prepared CD powder was dispersed in 25 mL of the mixture of ammonium hydroxide (25 wt%) and hydrogen peroxide (30 wt%) in ratio 50:50 in a 100mL round bottom flask equipped with a condenser and the dispersion was heated to 80 °C and kept for 5 h. Even though no literature so far has explained why NH_4OH is used in the oxidization system, hereby we think the presence of NH_4OH acted as a controlled-release agent to prevent sharp reaction between H_2O_2 and carbon dots. After that, the resulting dispersion was dialyzed with 0.5-1 kD membrane against distilled water for 3 days until the pH of buffer solution dropped to natural. The remaining solution was then collected and freeze dried for future characterization.

The reduction reaction with sodium borohydride was conducted based on the work in literature 14 with some modifications. Here, 0.2 g of sodium borohydride was added to a 1 g L^{-1} CD solution. Then, the pH was adjusted to ten with sodium hydroxide and the solution was refluxed for 6 h. Finally, the pH of the solution was decreased with hydrochloric acid and the suspension was collected, dialyzed and freeze dried to receive reduced CDs, hereby r-CDs.

Characterization:

TEM: the morphology of carbon dots was observed using a probe aberration-corrected analytical electron microscope JEOL ARM200F under STEM mode with operation voltage at 80 kV to prevent any beam damage on the carbon dots structure. Imaging condition: 12 cm condenser lens, 40 µm C12 aperture with 3 mm bright field aperture.

Raman: Room temperature nonpolarized Raman spectra of the samples were obtained in the backscattering geometry with a Horiba T64000 Raman system. Suitable edge filter for the 488 nm line of a Coherent Innoca Spectrum 70C Ar^+-Kr^+ laser is used with the system.

FTIR measurements: Fourier Transform Infrared Spectroscopy (FTIR) spectra were recorded with freeze dried CD powder by using a Bruker Tensor 27 instrument equipped with diamond lens Attenuated Total Reflectance (ATR) module in the range from 4000 cm^{-1} to 400 cm^{-1}.

XPS measurements: the XPS was performed using an AXIS Ultra DLD (Kratos Surface Analysis) setup equipped with an 180° hemispherical analyser, using Al $K\alpha_1$ (1486.74 eV) radiation produced by a monochromatized X-Ray source at operating power of 300 W (15 kV × 20 mA).

Continuous-wave EPR measurements were performed on a Bruker E-scan benchtop spectrometer at room temperature. Experimental parameters were as follow: microwave frequency ~9.773 GHz, 2 mW microwave power, 0.15 mT modulation amplitude, 86 kHz modulation frequency, 81.92 ms conversion time and 20.48 ms time constant.

Pulsed EPR measurements were performed using an X/Q-band Bruker Elexsys E500 spectrometer equipped with a closed-cycle cryostat (Cryogenic Ltd., UK). Depending on the amount of sample available either an ER 4118X-MS2 (9.4638 GHz, o-CDs) or an ER 4118X-MD5 (9.6585 GHz, HTC- and r-CQDs) resonator was used.

Two-pulse echo-detected field sweeps (EDFS) were acquired with the pulse sequence $\pi/2-\tau-\pi-\tau-$echo ($\pi/2$ = 16 ns, π = 32, and τ = 200 ns). HYSCORE spectra were recorded with the 4-pulse sequence $\pi/2-\tau-\pi/2-t1-\pi-t2-\pi/2-\tau-$echo; $\pi/2$ = 16 ns, π = 16 ns at twice the power of the $\pi/2$ pulses, initial $t_1 = t_2$ = 80 ns, time increment 20 ns, τ given in figure legends, 8-step phase cycle, number of points 100 x 100.

In an effort to minimise the drawback of blind spots a series of HYSCORE spectra were measure for the HTC-CDs sample in the range 84 < τ < 384 ns, selected spectra are presented in the supplementary information file. All experiments were performed at room temperature.

Solid state ^{13}C CP-MAS NMR: All measurements were performed on an Agilent 850 MHz (19.97T) solid state NMR-spectrometer resonant at 849.709 MHz for protons and 213.664 MHz for ^{13}C. Chemical shifts were referenced to TMS using adamantane as a secondary reference at 38.48 ppm. A 3.2 mm T3 design probe was used spinning at the magic angle with a spinning speed of 4 kHz. The acquisition time was set to 8 ms and the recycle delay set to 3 s for all samples and 4 s for o-CDs. To

enhance the ^{13}C signal, linearly ramped cross polarization from hydrogen to carbon was used with a contact time of 1 ms. The B1 field strengths were set to 60 kHz for both nuclei. Proton Spinal decoupling with a rf field strength of 110 kHz at a pulse width of 5 µs and a phase of 14o was used. A 2D-PASS sequence[70] with a pitch of 32 and cogwheel phase cycling was used to acquire spinning sideband free spectra by shearing the data and summing over the center band and all spinning sidebands as to not lose any signal intensity.

Steady-state optical spectroscopy: UV/Vis was measured using Perkin Elmer Lambda LS 35 instrument and PL spectra using Perkin Elmer LS55 instrument with excitations from 250 nm to 530 nm in 20 nm increments. Solutions for these were prepared with deionized water and concentrations were kept at 0.1 mg/ml. Photoluminescence quantum yield (Φ) of carbon dots was determined at 370 nm excitation by using quinine sulphate (QS) as a reference and following the procedure as described by Miller et al.[71]

Transient Absorption Spectroscopy (TAS): measurement was carried our using a Solstice Ti:Sapphire regenerative amplifier of Newport corporation. The output of the laser was 1 kHz, 800 nm, 92 fs pulses which were split with a partly-reflective mirror and the two beams used for pump and probe pulse generation. The excitation pump pulses were generated with TOPAS-NIRUVIS (Light Conversion) and the probe pulses with a sapphire crystal. Transient absorption spectrometer (Ultrafast Systems) with a 6 ns delay stage and detection using CMOS arrays. The CDs were studied using 1 mm cuvette filled in ambient air and using 310 nm and 360 nm excitation pulses with varied intensities.

Time Correlated Single Photon Counting (TCSPC): experiments were carried with LifeSpec II (Edinburgh Instruments Ltd.) using 405 nm 60 ps pulsed laser diode for excitation in an ambient atmosphere using 1 mm cuvette.

Acknowledgements

H. Luo thanks the Chinese government for the award of CSC scholarships. SD is grateful for financial support by Edinburgh Instruments. This work is part-funded by the European regional Development Fund through the Welsh Government. We thank the Diamond Light Source for access and support in use of the electron Physical Science Imaging Centre (Instrument E01 proposal EM17587) that contributed to the results presented here. Support from the Dutch organization for scientific research (NWO) for the solid-state NMR facility for advanced materials science in Nijmegen, which is part of the uNMR-NL consortium, is gratefully acknowledged.

Conflict of interest

The authors declare no conflict of interest.

Keywords: carbon dots, nanostructures, fluorescence, mechanism, laser spectroscopy

[1] X. Xu, R. Ray, Y. Gu, H. J. Ploehn, L. Gearheart, K. Raker, W. A. Scrivens, *J. Am. Chem. Soc.* **2004**, *126*, 12736–12737.

[2] M. Han, S. Zhu, S. Lu, Y. Song, T. Feng, S. Tao, J. Liu, B. Yang, *Nano Today* **2018**, *19*, 201–218.

[3] S. N. Baker, G. A. Baker, *Angew. Chemie - Int. Ed.* **2010**, *49*, 6726–6744.

[4] R. Wang, K.-Q. Lu, Z.-R. Tang, Y.-J. Xu, *J. Mater. Chem. A* **2017**, *5*, 3717–3734.

[5] G. A. M. Hutton, B. C. M. Martindale, E. Reisner, *Chem. Soc. Rev.* **2017**, *46*, 6111–6123.

[6] P. G. Luo, S. Sahu, S.-T. Yang, S. K. Sonkar, J. Wang, H. Wang, G. E. LeCroy, L. Cao, Y.-P. Sun, *J. Mater. Chem. B* **2013**, *1*, 2116–2127.

[7] S. Y. Lim, W. Shen, Z. Gao, *Chem. Soc. Rev.* **2015**, *44*, 362–381.

[8] Y. Wang, A. Hu, *J. Mater. Chem. C* **2014**, *2*, 6921–6939.

[9] M. L. Liu, B. Bin Chen, C. M. Li, C. Z. Huang, *Green Chem.* **2019**, *21*, 449–471.

[10] S. Kellici, J. Acord, K. E. Moore, N. P. Power, V. Middelkoop, D. J. Morgan, T. Heil, P. Coppo, I.-A. Baragau, C. L. Raston, *React. Chem. Eng.* **2018**, *3*, 949–958.

[11] Y. Dong, J. Shao, C. Chen, H. Li, R. Wang, Y. Chi, X. Lin, G. Chen, *Carbon N. Y.* **2012**, *50*, 4738–4743.

[12] H. Nie, M. Li, Q. Li, S. Liang, Y. Tan, L. Sheng, W. Shi, S. X. A. Zhang, *Chem. Mater.* **2014**, *26*, 3104–3112.

[13] L. Pan, S. Sun, A. Zhang, K. Jiang, L. Zhang, C. Dong, Q. Huang, A. Wu, H. Lin, *Adv. Mater.* **2015**, *27*, 7782–7787.

[14] V. Strauss, J. T. Margraf, C. Dolle, B. Butz, T. J. Nacken, W. Bauer, W. Peukert, E. Spiecker, T. Clark, D. M. Guldi, *J. Am. Chem. Soc.* **2014**, *49*, 17308–17316.

[15] J. T. Margraf, V. Strauss, D. M. Guldi, T. Clark, *J. Phys. Chem. B* **2015**, *119*, 7258–7265.

[16] S. Zhu, Y. Song, X. Zhao, J. Shao, J. Zhang, B. Yang, *Nano Res.* **2015**, *8*, 355–381.

[17] D. Pan, J. Zhang, Z. Li, C. Wu, X. Yan, M. Wu, *Chem. Commun.* **2010**, *46*, 3681–3683.

[18] Y. P. Sun, B. Zhou, Y. Lin, W. Wang, K. A. S. S. Fernando, P. Pathak, M. J. Meziani, B. A. Harruff, X. Wang, H. Wang, et al., *J. Am. Chem. Soc.* **2006**, *128*, 7756–7757.

[19] M. Fu, F. Ehrat, Y. Wang, K. Z. Milowska, C. Reckmeier, A. L. Rogach, J. K. Stolarczyk, A. S. Urban, J. Feldmann, *Nano Lett.* **2015**, *15*, 6030–6035.

[20] B. Zhu, S. Sun, Y. Wang, S. Deng, G. Qian, M. Wang, A. Hu, *J. Mater. Chem. C* **2013**, *1*, 580–586.

[21] A. Marinovic, L. S. Kiat, S. Dunn, M. M. Titirici, J. Briscoe, *ChemSusChem* **2017**, *10*, 1004–1013.

[22] X. Zhang, M. Jiang, N. Niu, Z. Chen, S. Li, S. Liu, J. Li, *ChemSusChem* **2018**, *11*, 11–24.

[23] N. Papaioannou, A. Marinovic, N. Yoshizawa, A. E. Goode, M. Fay, A. Khlobystov, M. Titirici, A. Sapelkin, *Sci. Rep.* **2018**, *8*, 6559.

[24] A. C. Ferrari, J. Robertson, *Phys. Rev. B* **2000**, *61*, 14095–14107.

[25] B. C. M. Martindale, G. A. M. Hutton, C. A. Caputo, S. Prantl, R. Godin, J. R. Durrant, E. Reisner, *Angew. Chemie - Int. Ed.* **2017**, *56*, 6459–6463.

[26] C. V. V Pham, M. Krueger, M. Eck, S. Weber, E. Erdem, *Appl. Phys.*

Lett. **2014**, *104*, 3–8.

[27] G. Sandeep Kumar, R. Roy, D. Sen, U. K. Ghorai, R. Thapa, N. Mazumder, S. Saha, K. K. Chattopadhyay, *Nanoscale* **2014**, *6*, 3384–3391.

[28] M. C. Ortega-Liebana, N. X. Chung, R. Limpens, L. Gomez, J. L. Hueso, J. Santamaria, T. Gregorkiewicz, *Carbon N. Y.* **2017**, *117*, 437–446.

[29] Z. Zhang, J. Zhang, N. Chen, L. Qu, *Energy Environ. Sci.* **2012**, *5*, 8869–8890.

[30] Y. Wang, S. Kalytchuk, Y. Zhang, H. Shi, S. V. Kershaw, A. L. Rogach, *J. Phys. Chem. Lett.* **2014**, *5*, 1412–1420.

[31] M. Sudolská, M. Dubecký, S. Sarkar, C. J. Reckmeier, R. Zbořil, A. L. Rogach, M. Otyepka, *J. Phys. Chem. C* **2015**, *119*, 13369–13373.

[32] G. Eda, Y. Y. Lin, C. Mattevi, H. Yamaguchi, H. A. Chen, I. S. Chen, C. W. Chen, M. Chhowalla, *Adv. Mater.* **2010**, *22*, 505–509.

[33] Y. Zhou, Q. Bao, L. A. L. Tang, Y. Zhong, K. P. Loh, *Chem. Mater.* **2009**, *21*, 2950–2956.

[34] G. Eda, M. Chhowalla, *Adv. Mater.* **2010**, *22*, 2392–2415.

[35] R. Y. N. Gengler, D. S. Badali, D. Zhang, K. Dimos, K. Spyrou, D. Gournis, R. J. D. Miller, *Nat. Commun.* **2013**, *4*, 1–5.

[36] F. Ehrat, S. Bhattacharyya, J. Schneider, A. Löf, R. Wyrwich, A. L. Rogach, J. K. Stolarczyk, A. S. Urban, J. Feldmann, *Nano Lett.* **2017**, *17*, 7710–7716.

[37] L. Đorđević, F. Arcudi, A. D'Urso, M. Cacioppo, N. Micali, T. Bürgi, R. Purrello, M. Prato, *Nat. Commun.* **2018**, *9*, 3442.

[38] S. Zhu, Q. Meng, L. Wang, J. Zhang, Y. Song, H. Jin, K. Zhang, H. Sun, H. Wang, B. Yang, *Angew. Chemie - Int. Ed.* **2013**, *52*, 3953–3957.

[39] Y. Yang, J. Cui, M. Zheng, C. Hu, S. Tan, Y. Xiao, Q. Yang, Y. Liu, *Chem. Commun.* **2012**, *48*, 380–382.

[40] Q. Liang, W. Ma, Y. Shi, Z. Li, X. Yang, *Carbon N. Y.* **2013**, *60*, 421–428.

[41] S. Sahu, B. Behera, T. K. Maiti, S. Mohapatra, *Chem. Commun.* **2012**, *48*, 8835–8837.

[42] X. Zhao, S. Lu, S. Zhu, Y. Song, B. Yang, *Nano Today* **2015**, *11*, 128–132.

[43] S. H. Song, M.-H. Jang, J. Chung, S. H. Jin, B. H. Kim, S.-H. Hur, S. Yoo, Y.-H. Cho, S. Jeon, *Adv. Opt. Mater.* **2014**, *2*, 1016–1023.

[44] S. Ghosh, A. M. Chizhik, N. Karedla, M. O. Dekaliuk, I. Gregor, H. Schuhmann, M. Seibt, K. Bodensiek, I. A. T. Schaap, O. Schulz, et al., **2014**, *14*, 5656–5661.

[45] S. Dey, S. Zhang, X. Ma, Y. Meng, L. Zhang, J. Zhao, X. Sun, Y. Lei, J. He, *J. Mater. Chem. A* **2016**, *4*, 4161–4171.

[46] Y. Song, S. Zhu, S. Zhang, Y. Fu, L. Wang, X. Zhao, B. Yang, *J. Mater. Chem. C* **2015**, *3*, 5976–5984.

[47] L. Wang, S. J. Zhu, H. Y. Wang, S. N. Qu, Y. L. Zhang, J. H. Zhang, Q. D. Chen, H. L. Xu, W. Han, B. Yang, et al., *ACS Nano* **2014**, *8*, 2541–2547.

[48] L. Sui, W. Jin, S. Li, D. Liu, Y. Jiang, A. Chen, H. Liu, Y. Shi, D. Ding, M. Jin, *Phys. Chem. Chem. Phys.* **2016**, *18*, 3838–3845.

[49] C. Galande, A. D. Mohite, A. V Naumov, W. Gao, L. Ci, A. Ajayan, H. Gao, A. Srivastava, R. B. Weisman, P. M. Ajayan, *Sci. Rep.* **2011**, *1*, 85.

[50] M. O. Dekaliuk, O. Viagin, Y. V. Malyukin, A. P. Demchenko, *Phys. Chem. Chem. Phys.* **2014**, *16*, 16075–16084.

[51] B. Ghosh, M. Takeguchi, J. Nakamura, Y. Nemoto, T. Hamaoka, S. Chandra, N. Shirahata, *Sci. Rep.* **2016**, *6*, 36951.

[52] V. Strauss, A. Kahnt, E. M. Zolnhofer, K. Meyer, H. Maid, C. Placht, W. Bauer, T. J. Nacken, W. Peukert, S. H. Etschel, et al., *Adv. Funct. Mater.* **2016**, *26*, 7975–7985.

[53] M. Righetto, A. Privitera, I. Fortunati, D. Mosconi, M. Zerbetto, M. L. Curri, M. Corricelli, A. Moretto, S. Agnoli, L. Franco, et al., *J. Phys. Chem. Lett.* **2017**, *8*, 2236–2242.

[54] R. Kirmse, *Magn. Reson. Chem.* **1995**, *33*, 698.

[55] S. Qu, D. Zhou, D. Li, W. Ji, P. Jing, D. Han, L. Liu, H. Zeng, D. Shen, *Adv. Mater.* **2016**, *28*, 3516–3521.

[56] F. Lin, D. Pei, W. He, Z. Huang, Y. Huang, X. Guo, *J. Mater. Chem.* **2012**, *22*, 11801–11807.

[57] A. Jaiswal, S. S. Ghosh, A. Chattopadhyay, *Chem. Commun.* **2012**, *48*, 407–409.

[58] X. Wang, K. Qu, B. Xu, J. Ren, X. Qu, *Nano Res.* **2011**, *4*, 908–920.

[59] L. Wang, S. J. Zhu, H. Y. Wang, Y. F. Wang, Y. W. Hao, J. H. Zhang, Q. D. Chen, Y. L. Zhang, W. Han, B. Yang, et al., *Adv. Opt. Mater.* **2013**, *1*, 264–271.

[60] X. Wen, P. Yu, Y. R. Toh, X. Hao, J. Tang, *Adv. Opt. Mater.* **2013**, *1*, 173–178.

[61] P. George, J. Strait, J. Dawlaty, S. Shivaraman, M. Chandrashekhar, F. Rana, M. G. Spencer, *Nano Lett* **2008**, *8*, 17–20.

[62] J. M. Dawlaty, S. Shivaraman, M. Chandrashekhar, F. Rana, M. G. Spencer, *Appl. Phys. Lett.* **2008**, *92*, 042116.

[63] P. Chen, F. Wang, Z. F. Chen, Q. Zhang, Y. Su, L. Shen, K. Yao, Y. Liu, Z. Cai, W. Lv, et al., *Appl. Catal. B Environ.* **2017**, *204*, 250–259.

[64] Y. Li, Z. Liu, Y. Wu, J. Chen, J. Zhao, F. Jin, P. Na, *Appl. Catal. B Environ.* **2018**, *224*, 508–517.

[65] J. Briscoe, A. Marinovic, M. Sevilla, S. Dunn, M. Titirici, *Angew. Chemie - Int. Ed.* **2015**, *54*, 4463–4468.

[66] N. Baccile, G. Laurent, C. Coelho, F. Babonneau, L. Zhao, M.-M. Titirici, *J. Phys. Chem. C* **2011**, *115*, 8976–8982.

[67] M.-M. Titirici, M. Antonietti, N. Baccile, *Green Chem.* **2008**, *10*, 1204.

[68] N. Baccile, G. Laurent, F. Babonneau, F. Fayon, M.-M. Titirici, M. Antonietti, *J. Phys. Chem. C* **2009**, *113*, 9644–9654.

[69] G. Tsilomelekis, M. J. Orella, Z. Lin, Z. Cheng, W. Zheng, V. Nikolakis, D. G. Vlachos, *Green Chem.* **2016**, *18*, 1983–1993.

[70] N. Ivchenko, C. E. Hughes, M. H. Levitt, *J. Magn. Reson.* **2003**, *164*, 286–293.

[71] A. T. R. Williams, S. A. Winfield, J. N. Miller, *Analyst* **2004**, *108*, 1067–1071.

[72] S. R. Singamaneni, A. Stesmans, J. Van Tol, D. V. Kosynkin, J. M. Tour, *AIP Adv.* **2014**, *4*, 047104.

Entry for the Table of Contents

FULL PAPER

This paper aims to study the structural evolution of hydrothermal carbon dots after oxidation and reduction and demonstrate how fine tuning the structure can dramatically change optical properties. The in-depth spectroscopic analysis identifies the dynamics of photoluminescence, allowing the authors to fully resolve the relaxation pathways in these carbon dots.

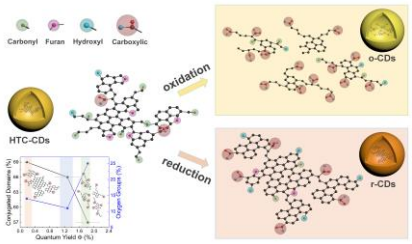

Hui Luo, Nikolaos Papaioannou, Enrico Salvadori, Maxie Roessler, Gereon Ploenes, Ernst R. H. van Eck, Liviu Tanase, Jingyu Feng, Yiwei Sun, Yan Yang, Mohsen Danaie, Ana Belem Jorge Sobrido, Andrei Sapelkin, James Durrant, Stoichko D. Dimitrov and Maria-Magdalena Titirici**

Page No. – Page No.

Manipulating the optical properties of carbon dots via fine tuning their structural features